Uranyl ($\mathrm{UO_2}^{2+}$) Structuring and Dynamics at Graphene/Electrolyte Interface

Nitesh Kumar[a,*]
[a] *Department of Chemistry, Washington State University, Pullman, Washington 99163, United States,*
[*] *E-mail: nitesh.kumar@wsu.edu, kmnitesh05@gmail.com*

(Dated: October 7, 2024)

The physicochemical phenomena at the solid/electrolyte interfaces govern various industrial processes ranging from energy generation, storage, and catalysis to chemical separations and purification. Adsorption-based solid/liquid extraction methods are promising for the selective and rapid separation of nuclear (such as uranium) and other critical materials. In this study, we quantified the adsorption, complexation, and dynamics of $\mathrm{UO_2}^{2+}$ ions on the graphene surface in various electrolyte media ($\mathrm{LiNO_3}$, $\mathrm{NaNO_3}$ and $\mathrm{CsNO_3}$) using all-atom molecular dynamics simulations, in combination with network theory based subensemble analysis, enhanced sampling, and temporal analysis. We observe that the choice of background electrolyte impacts the propensity of $\mathrm{UO_2}^{2+}$ adsorption on the graphene surface, with $\mathrm{LiNO_3}$ being the most favorable at both low and high uranyl-nitrate concentrations. Even though $\mathrm{UO_2}^{2+}$ primarily retained its coordination with water and interacted via the outer-sphere mechanism with graphene, the interfacial segregation of $\mathrm{NO_3}^-$ increased the number of contact ion pairs (CIP) between $\mathrm{UO_2}^{2+}$ and $\mathrm{NO_3}^-$ ions, and the residence times of $\mathrm{UO_2}^{2+}$ within the interfacial region. This study provides a fundamental understanding of the structure and dynamics of $\mathrm{UO_2}^{2+}$ on the solid surfaces necessary to design advanced adsorption-based separation methods for energy-relevant materials.

Keywords: Graphene, Electronic Continuum Correction, Network Theory, Solid-Liquid Interface, Molecular Adsorption, Chemical Separation and Free Energy.

I. INTRODUCTION

U^{6+} generally present as uranyl ($\mathrm{UO_2}^{2+}$) ions in aqueous media is one of the most common radionuclides present in nuclear waste and seawater.[1–3] Multiple separation techniques, such as liquid/liquid extraction, ion exchange, membrane processing, supramolecular extraction, etc., have been used for the selective extraction of the $\mathrm{UO_2}^{2+}$ ions.[4–8] With advances in adsorption-based separation methods, graphene, and its functionalized forms are now considered promising adsorbents for the separation of $\mathrm{UO_2}^{2+}$ even at low concentrations.[9–14] However, a detailed understanding of the chemistry associated with $\mathrm{UO_2}^{2+}$ adsorption, complexation, and dynamics at the graphene/electrolyte surface is lacking. Recent developments reveal ion adsorption at biphasic interfaces to be independent of the Hofmeister trend.[15, 16] As such, Cole et al. showed segregation of both $\mathrm{H_3O^+}$ and $\mathrm{OH^-}$ ions at the graphene/aqueous interface following surfactant-like behavior.[17] Jungwirth and Tobias showed the favorability of large polarizable halide ions such as $\mathrm{I^-}$ and $\mathrm{Br^-}$ (with loose water coordination) over smaller ones ($\mathrm{Cl^-}$ and $\mathrm{F^-}$) for adsorption at liquid/liquid interfaces.[18–20] A recent study of $\mathrm{UO_2}^{2+}$ at the hexane/$\mathrm{LiNO_{3(aq)}}$ interface revealed an increased uranyl complexation with nitrate to form mono- or dinitrate uranyl···nitrate complexes. The residence times of $\mathrm{UO_2}^{2+}$ within the interfacial region were longer compared to the bulk aqueous phase, and further increased with higher $\mathrm{LiNO_3}$ concentrations. This suggests that $\mathrm{NO_3}^-$ ions cooperatively influence the interfacial behavior of $\mathrm{UO_2}^{2+}$ ions.[21] However, the effects of counterion cooperativity on adsorption at solid interfaces like functionalized graphene/electrolyte are not well understood, including how favorable $\mathrm{NO_3^-}$ adsorption[22, 23] and ion gradients influence $\mathrm{UO_2^{2+}}$ co-adsorption, complexation and dynamic at the pure graphene/electrolyte interface.[24]

Polarization of ions, especially at the graphene surface, affects the adsorption and dynamics in the interfacial region. Accurate modeling of the adsorption behavior of actinide ions requires the inclusion of polarization effects either explicitly or implicitly within the force fields.[25] One of the methods is to construct system-specific polarizable force fields for ions, water, and graphene. However, the parameterization of the polarizable force fields for concentrated electrolyte systems is computationally expensive and time-consuming. Various methods have been used to indirectly account for polarization effects, such as including polarizability only to ions,[17, 26] or optimizing ion-graphene (ion-π) interactions by tuning the Lennard-Jones ($\epsilon_{i\text{-}c}$) parameter based on the DFT free energies of adsorption and charge transfer.[27] Recent studies have accounted for the electronic polarization effects using Electronic Continuum Correction (ECC) methodology that involves scaling of the ion charges (q_i) in the nonbonded potential terms of the nonpolarizable models.[28] The ECC methodology is extensively benchmarked with experiments and has improved bulk and interfacial properties compared to traditional nonpolarizable force fields.[28] Therefore, we utilized ECC UO_2^{2+}/nitrate force fields, optimized to reproduce the experimental first and second uranyl-nitrate association constants, K_1 and K_2, in 1-5 M $LiNO_3$ solutions.[20, 28] Moreover, the amber force fields in combination with the TIP3P water model showed a similar distribution of water at the graphene surface as observed using *ab initio* molecular dynamics simulations.[29]

Extensive efforts have been dedicated to understanding the behavior of ions and other molecules at solid/liquid interfaces through experimental techniques such as Vibrational Sum Frequency Generation (VSFG) or X-ray scattering, alongside atomistic simulations.[30–37] However, these characterizations often focus on ensemble-averaged properties. The radioactive nature of uranium further complicates experimental design. Thus, molecular dynamics simulations are crucial for providing detailed microscopic insights into ion behavior at interfaces, guiding experimental setup, and analyses. Using subensemble analysis with network theory, enhanced sampling, and temporal analysis, we characterize the microscopic behavior of uranyl ions at the graphene surface, providing details typically inaccessible with current experimental techniques. Herein, we employed all-atom molecular dynamics simulations to investigate the impact of different nitrate-based electrolyte media on adsorption, complexation, and dynamics of UO_2^{2+} at the graphene/electrolyte interface. To the best of our knowledge, this study represents the first detailed characterization of uranyl behavior at a pure graphene/electrolyte interface. Here, we compared UO_2^{2+} adsorption in various electrolyte mediums, such as $LiNO_3$, $NaNO_3$, and $CsNO_3$, and with low and high uranyl-nitrate concentrations to understand the impact of background electrolyte on the adsorption behavior of UO_2^{2+} at the graphene surface. We utilized NO_3^- in combinations with alkali metal ions, owing to the frequent use of uranyl salts in nitrate media. UO_2^{2+} is observed to adsorb favorably in the interfacial region of the graphene/electrolyte surface. Its density is affected by the choice of background electrolyte, influencing its residence times at the interface. Hydration-mediated ion-graphene interactions in combination with NO_3^- cooperativity, as a result of anionic excess, collectively impact UO_2^{2+} adsorption propensity and complexation in the interfacial region.

II. RESULTS AND DISCUSSION

A. ***Cooperative adsorption, orientation, and dynamics***

The UO_2^{2+} adsorption behavior at the graphene/electrolyte interface at both low (0.36 M) and high (1.08 M) uranyl-nitrate concentration is characterized using the normalized density profiles along the z axis as

$$\rho_\alpha(z) = \frac{\sum_{i\in\alpha}\delta(z_i - z)}{\rho_b}, \tag{1}$$

where δ is the Dirac delta function, the sum is applied to all atoms i. ρ_b is the number density in the bulk aqueous phase. The z-position of the graphene sheet is used as a reference point (z_0). At the low uranyl-nitrate concentration of 0.36 M, we observe a UO_2^{2+} excess with a density of almost 45 to 60× in the interfacial region (ranging from 2 to 8 Å) relative to the bulk, depending on the choice of background electrolyte. The highest density of interfacial UO_2^{2+} is obtained in the system with $LiNO_3$, favoring UO_2^{2+} adsorption to the extent of 60× more relative to the bulk. Interestingly, the adsorption propensity of UO_2^{2+} was inversely correlated with the radii of the cation of the background electrolyte as ($LiNO_3 > NaNO_3 > CsNO_3$), with a respective increase of almost 60%, 55%, & 45% relative to the bulk (Figure 1). At higher uranyl-nitrate concentration of 1.08 M, a UO_2^{2+} density in the interfacial region is $\sim 15 \times$ higher than in the bulk.

Interestingly, we observe a shift in the location of UO_2^{2+} density maxima for different electrolytes. The maximum of the UO_2^{2+} density in the $LiNO_3$ system is found closer to the graphene surface than in the $CsNO_3$ system (Figure 1). This shift is associated with the ability of Cs^+ ions to lose their coordinated water, resulting in a higher density of Cs^+ near the graphene surface compared to Li^+ ions. Consequently, this increases competition for UO_2^{2+} ions to adsorb near the graphene surface. We infer that the enhanced density of UO_2^{2+} on the graphene surface is a collective result of the interactions of UO_2^{2+} with the graphene surface as a result of outer-sphere ion-π interactions mediated by the interfacial water and the cooperativity by the adsorbed NO_3^- ions.

To understand the ion enrichment in the interfacial region **I**, we calculated the surface excess Γ_i as

$$\Gamma_i = \int_{z_0}^{z'} dz \left(\frac{\rho_i(z)}{\rho_i^b} - 1 \right)$$

where $\rho_\mathrm{i}(\mathrm{z})$ and $\rho_\mathrm{i}{}^\mathrm{b}$ are the density of ions along the z axis and in the bulk, respectively. z_0 is the z position

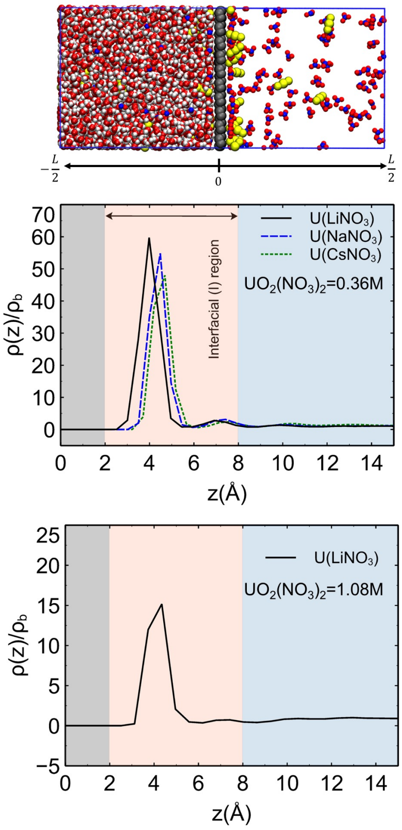

FIG. 1: Simulation snapshot illustrating the adsorption of ${UO_2}^{2+}$ (yellow) at the graphene/electrolyte interface (Upper panel). Oxygen (O), nitrogen (N), and carbon (C) atoms are shown in red, blue, and grey colors respectively. H_2O between 0 and L/2 are hidden for visual clarity. The normalized density profiles (ρ_z) of ${UO_2}^{2+}$ along the z axis in various 1.41 M electrolytic systems ($LiNO_3$, $NaNO_3$ and $CsNO_3$) and 0.36 M $UO_2(NO_3)_2$ (Middle panel) and 1.08 M $UO_2(NO_3)_2$ (Lower panel). The densities are normalized by the bulk ${UO_2}^{2+}$ density ρ_b. Graphene, interfacial (**I**), and bulk regions are shown in grey, pink, and blue respectively.

of the graphene sheet, $z^{'}$ is the upper limit of the region S_2, i.e., $z_{S_2} = 8$ Å. The values of Γ_i are directly correlated with the enhancement of the ions in the interfacial region (S_1 and S_2 as shown in Figure 2). In each system, ${NO_3}^-$ showed a substantial enhancement compared to alkali metal ions M^+ (Figure 2). Interestingly, the surface excess of ${UO_2}^{2+}$ followed the same trend as ${NO_3}^-$, that is, ($LiNO_3$ >, $NaNO_3$ >, $CsNO_3$), showing cooperativity in adsorption behavior. The excess of ${NO_3}^-$ attracted ${UO_2}^{2+}$, causing an increase in the concentration gradient of ${UO_2}^{2+}$ at the interface. The Γ_i of the interfacial M^+ followed the ion charge density trend i.e., $Cs^+ > Na^+ > Li^+$. The $\Gamma_i(M^+)$ trend correlates with the ability of cations to lose water coordination in the interfacial region. The extent of cooperative ${NO_3}^-$ effects on ${UO_2}^{2+}$ will decrease due to competition by Cs^+ ions for surface adsorption.[38] As such, the relatively higher density and competition from the Cs^+ ions at the interface created a screening layer and made it difficult for ${NO_3}^-$ and UO_2^{2+} to adsorb directly on the graphene surface, as illustrated by a lower density of ${NO_3}^-$ or ${UO_2}^{2+}$ in the system with Cs^+ relative to Li^+ (Figure 2 Right panel).

Next, we present the orientation distribution of the $\overrightarrow{UO}$ vector along a unit vector perpendicular to the graphene surface (as shown in the inset of Figure 3) in the interfacial and bulk regions. Angles 0° and 90° represent the respective perpendicular and parallel orientations relative to the graphene surface. A high probability of $\cos\theta \geq 0.5$ or ≤ -0.5 shows a favorability of the orientation of ${UO_2}^{2+}$ perpendicular to the graphene sheet. Therefore, the highest probability of orientation of ~ 0.7 shows its preferable orientation at $\sim 45°$. Greathouse et al. reported a ${UO_2}^{2+}$ orientation of $\sim 45°$ at the surface of quartz (101).[39] Interestingly, the choice of background electrolyte has only a minor effect on the orientation of interfacial ${UO_2}^{2+}$.

To characterize the role of the increased density of interfacial ${UO_2}^{2+}$ on its interfacial dynamics, we quantified the ${UO_2}^{2+}$ residence in the interfacial regions by calculating the average time spent in the given slab of size 2 Å.[21] The survival probability is given by

$$P(t) = \frac{N(t, \Delta t)}{\sum_t N(t, \Delta t)} \tag{2}$$

$N(t, \Delta t)$ is the continuous-time duration of the ions in the respective slabs. The average residence time τ is computed as

$$\tau = \int_0^\infty tP(t)dt, \tag{3}$$

${UO_2}^{2+}$ residence time, $\tau({UO_2}^{2+})$, in various interfacial slabs is shown in Table S1. On average, ${UO_2}^{2+}$ spent ~ 590 ps at the graphene/electrolyte interface compared to 86.64 ps on an analogous hexane surface with a similar system composition using $LiNO_3$ as the background electrolyte.[21] A $\sim 7\times$ increase in τ at the graphene compared to the hexane interface clearly shows the favorability of ${UO_2}^{2+}$ for the graphene surface adsorption primarily due to favorable adsorption of uranyl at graphene/electrolyte interface.[21]

B. *Ion complexation at the graphene surface*

To understand how the ion concentration gradient alters ${UO_2}^{2+}$ complexation with ${NO_3}^-$ at the

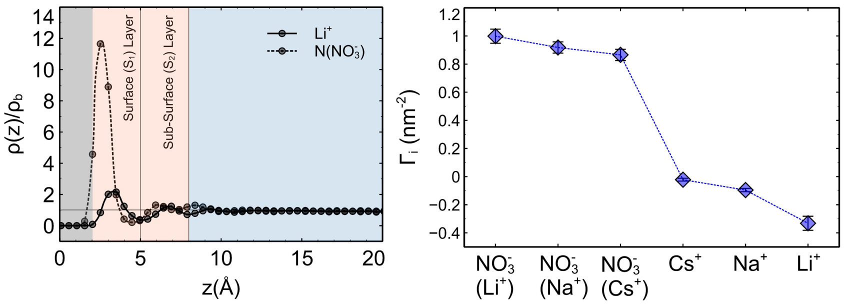

FIG. 2: The normalized density profiles of Li^+ and $NO_3{}^-$ (ρ_z) along the z axis (Left panel). The surface excess Γ_i of ions at the graphene/electrolyte interface (Right panel). The interfacial region **I** ranging from 2 to 8 Å is divided into two sublayers, S_1 (2-5 Å) and S_2 (5-8 Å), based on layering formed by the background electrolyte as shown in the left panel.

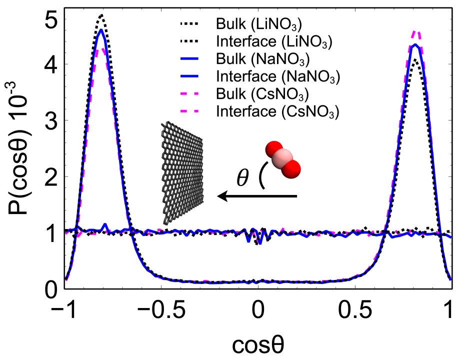

FIG. 3: The comparison of the $UO_2{}^{2+}$ orientation probability distributions in bulk and at the electrolyte/graphene interfacial region **I** with different electrolyte media. The error bars were computed using block averaging methodology. The definition of θ is provided in the inset.

graphene/electrolyte interface, the time-averaged number densities of individual $[UO_2(NO_3)_n]^{(2-n)+}$ ion pairs along the z axis are plotted in Figure 4. The computation of these profiles involved three major steps: (1) the creation of $UO_2{}^{2+}$-$NO_3{}^-$ connectivity networks, using r(U-NO) = 3.91 Å cutoff; (2) the characterization of $[UO_2(NO_3)_n]^{(2-n)+}$ complexes using the graph theory;[40, 41] (3) the binning of complex densities along the z-axis (bin size 0.2 Å, normalized by the volume of the bin) using the atomic coordinates of the U atoms involved in the $[UO_2(NO_3)_n]^{(2-n)+}$ complexes. The methodology is described in detail in ref 42. Experimental and computational studies revealed that $UO_2{}^{2+}$ interact strongly with five H_2O in the bulk aqueous phase under infinite dilution conditions.[43, 44] Within the electrolyte or acidic media, $UO_2{}^{2+}$ complex weakly with $NO_3{}^-$ to form $[UO_2(NO_3)]^+$ and $[UO_2(NO_3)_2]$ complexes with their respective association constants K_1 and K_2 in range 0.1-0.6 and 0.02-0.04 respectively.[21, 45–47] Interestingly, $UO_2{}^{2+}$ preserves its water coordination at the graphene surface, (Figure 4), resulting in outer-sphere interactions with the graphene surface. In the bulk and interfacial region, the five coordinated $[UO_2(NO_3)_0(H_2O)_5]^{2+}$ remained the most probable, followed by the mononitrate complexes. A similar trend is observed for the uranyl···nitrate complexation at the hexane/electrolyte interface.[21]

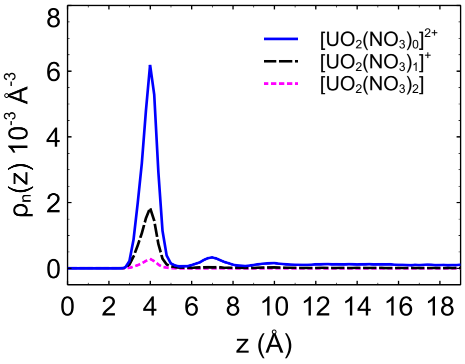

FIG. 4: Average number density $[UO_2(NO_3)_n]^{(2-n)+}$ (n=0, 2) complexes along the z axis in the system with $LiNO_3$.

Importantly, the propensity of $UO_2{}^{2+}$ complexes with $NO_3{}^-$ is higher for the graphene surface compared to the bulk, as revealed by the higher densities of both $[UO_2(NO_3)_1]^+$ and $[UO_2(NO_3)_2]$ complexes in the interfacial region (Figure 4). This increase is associated with the greater availability of nitrate ions for complexation, change in electrolyte concentration, and water structuring (*vide-infra*) near to the interface.

The impact of concentration gradients on the ion-pairing of the adsorbed Li^+ is studied in terms of $Li^+\cdots NO_3{}^-$ number density profiles along the z axis, using the graph theory approach analogous to the one used for $UO_2{}^{2+}$. The coordination of Li^+ with $NO_3{}^-$ is described using the distance of the first minima in the

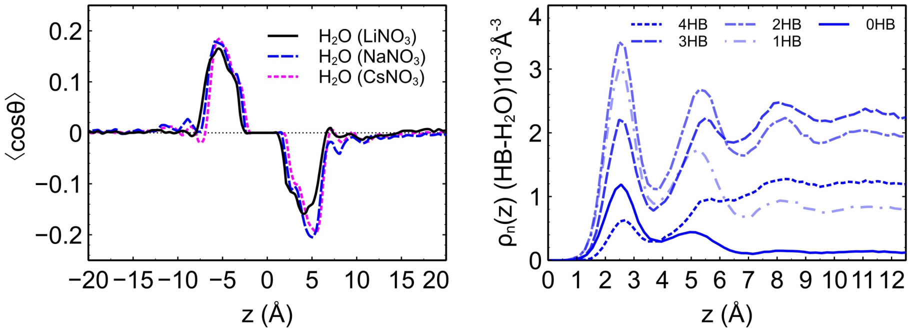

FIG. 5: (Left panel) Average dipole orientation profiles of H_2O along the z axis in various electrolyte media in the presence of ${UO_2}^{2+}$ ions. (Right panel) Average number densities of the H_2O in different H-bonding states along z axis in the electrolytic system with $LiNO_3$.

respective pair correlation functions, i.e. r_{cut} of 3.5 Å for $N(NO_3^-)$. Figure S2 shows the time-averaged number densities profiles of $[Li(NO_3)_n]^{(1-n)+}$ (n=0-1) complexes along the z axis. The results in Figure S2 show that unlike ${UO_2}^{2+}$, the interfacial concentration gradient alters the Li^+ solvation shell, causing an increase in the density of $LiNO_3$ CIPs near the graphene surface. It is revealed that the Li^+ present in the region S_1 showed enhanced density of CIPs compared to the region S_2 or the bulk aqueous phase. The enhanced ion···ion interactions of $Li^+ \cdots {NO_3}^-$ is related to ${NO_3}^-$ excess within the S_1 surface region.

C. ***Water structure and topology***

The average local structure of water at the dynamically evolving graphene/electrolyte interface is characterized using the orientation and the HB network of water in the interfacial region.[48, 49] The dipole orientation of water along the z axis is calculated using

$$\langle \cos(\theta_i) \rangle = \langle \sum_i \hat{\mu}_i \cdot \hat{\mathrm{n}}_z \rangle, \tag{4}$$

where, $\cos(\theta_\mathrm{i})$ is the angle between the unit H_2O dipole vector i, $\hat{\mu}_\mathrm{i}$ and a unit vector normal to the xy plane. The orientation of water in various electrolyte media is plotted in Figure 5. The water has an anisotropic orientation pattern in the surface region S_1 that extends to the subsurface region S_2. The average values of $\cos\theta \sim 0.2$ show a preferential parallel orientation of the water dipole vector along the surface normal vector, which is consistent with the cos values reported in the literature.[49, 50] The interfacial water molecules are oriented in such a way that the H atoms face the graphene surface and the O atoms face the bulk aqueous phase. The orientation of H_2O remained almost unaffected by the choice of electrolyte. Enhanced ion density in the interfacial region can alter the water HB network. The structure of water in the interfacial region has been studied in terms of changes in average HB with the change in the distance from the surface in $LiNO_3$ electrolyte media.[51] Layered distributions of average HB were reported for the water network as a result of dangling water molecules, which were correlated with the distribution of water density in the interfacial region.[50–52] Here, we report densities of various $(H_2O)_n$ HB along the z axis. H-bonding of water in the surface (S_1) sub-surface (S_2) region and bulk is compared using the average number density of water forming 1-5 HBs along the z axis. H-bonding network of H_2O is computed using combined distance and angle-based geometric criterion. HBs were defined based on O···H distance cutoff of 2.5 Å and an O···H-O angle in range 145-180°. The strong structure of water molecules in the vicinity of the graphene layer leads to dramatic variations in the HB pattern that range up to three interfacial layers of 3 Å. The highest population of water molecules in the S_1 & S_2 region formed 2 HB compared to the bulk, where the highest number of water formed 3 HB. More specifically, the water molecules present in the S_1 region formed HB in order $2 > 1 > 3 > 0 > 4 > 5$. Interestingly, the region S_1 contained a significant population of water molecules that did not form HB. The breakdown of the H-bonding network in S_1 and S_2 is directly linked to the stratified water structure in the interfacial region, which in turn is associated with the layered ion adsorption behavior observed at the graphene/electrolyte interface.

D. *Favorable interactions with graphene*

The adsorption affinity of $UO_2{}^{2+}$ and Li^+ towards graphene is studied using the potential of mean force simulations under infinite dilution conditions using one ion-pair (Figure 6). The z-distance between ion and graphene is used as the collective variable, as detailed in the SI. The presence of minima in the region 4-5 Å shows that the adsorption of $UO_2{}^{2+}$ is favored by outer-sphere (interfacial water-mediated) ion-graphene interactions. A wide and stable region is observed with a depth of -0.812 kcal/mol for the $UO_2{}^{2+}$ adsorption at the graphene surface. In comparison, the free energy for the Li^+ adsorption is observed to be -0.496 kcal/mol, the PMF of which exhibits a broad minimum, shifted to a smaller distance from the graphene surface (Figure 6). The $UO_2{}^{2+}$ interactions with graphene are more significant and longer than Li^+, persisting up to 15 Å from the surface of the graphene, as a result of stronger cation-π interactions accounted within the non-bonded parameters.[15] The increased density of $UO_2{}^{2+}$ in the **I** region correlates with the favorable free energy of adsorption. Therefore, the preferential adsorption of $UO_2{}^{2+}$ at graphene is a collective influence of thermodynamic stability and cooperation by the background electrolyte towards the $UO_2{}^{2+}$ adsorption at graphene.

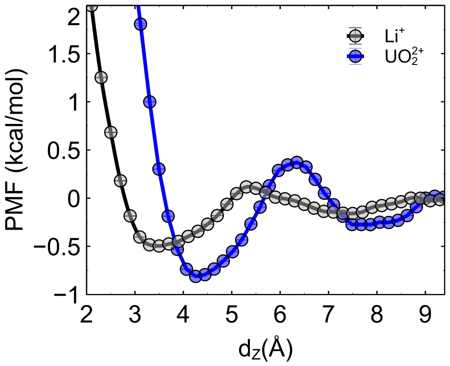

FIG. 6: Potential of mean forces (PMFs) of Li^+ and $UO_2{}^{2+}$ along the z-distance perpendicular to graphene (d_z). The collective variable d_z is described in the SI.

III. CONCLUSIONS

Molecular dynamics simulations were performed with ECC-optimized force fields to analyze the adsorption, complexation, and dynamics of $UO_2{}^{2+}$ ions at graphene/electrolyte interface under different electrolyte media ($LiNO_3$, $NaNO_3$, and $CsNO_3$). Our findings highlight that ion-graphene interactions, coupled with the type of background electrolyte, including favorable $NO_3{}^-$ graphene adsorption influence $UO_2{}^{2+}$ surface excess. Notably, $LiNO_3$ demonstrated the greatest efficacy in promoting $UO_2{}^{2+}$ adsorption. Specifically, electrolytes with the highest salting-out ability in the Hofmeister series result in the greatest uranyl adsorption. The potential of mean force simulations reveal that $UO_2{}^{2+}$ exhibit enhanced stability at the graphene interface relative to Li^+ ions. The cooperativity of $NO_3{}^-$ plays an important role in this process by increasing the residence times of uranyl, and the total number of CIPs between uranyl and nitrate ions in the interfacial region. In future work, exploring the role of electrolyte concentration and the choice of anions will provide a deeper understanding of how anions influence uranyl adsorption and dynamics near the graphene surface. The fundamental microscopic-level insights of uranyl adsorption, speciation, and dynamics presented in this study are crucial for developing effective adsorption-based techniques for selective uranyl separation from seawater or nuclear waste and guiding future separations research.

IV. MATERIALS AND METHODS

All-atom molecular dynamics simulations were performed using the GROMACS-2018.2 software package.[53] Initial systems composed of 5022 TIP3P H_2O, 130 M^+ (M^+ = Li^+, Na^+ & Cs^+) ions (1.41 M), 32 $UO_2{}^{2+}$, 194 $NO_3{}^-$ ions (0.36 M) and a graphene sheet were generated using the Packmol software package.[54] The ions and water molecules were randomly placed in an aqueous phase with dimensions 36.8 × 42.3 × 98.1 $Å^3$. Periodic boundary conditions were implemented in all three directions. Each system was equilibrated in NPT and NVT for 20 ns, followed by 40 ns production runs. Molecular dynamics were performed at 298 K using a leap-frog integrator with a 2 fs time step. The temperature selection aimed to replicate the conditions for uranyl extraction from seawater. However, other experimental conditions may require elevated temperatures. At elevated temperatures, variations in interfacial water structure and ion adsorption are anticipated, potentially increasing adsorption/desorption kinetics or weakening uranyl-nitrate complexation due to thermal fluctuations.Although the polarizability of water and graphene has a negligible effect on the structure and dynamics of water at the interface,[51] the presence of an electrolyte can create ion solvent polarization and graphene polarization. The polarizable force fields for heavy-metal ions and graphene are more computationally demanding than non-polarizable. To overcome cost barriers, Williams et al. [27] recently treated polarization effects by scaling Lennard-Jones parameters between graphene and ions. Alternatively, system polarization can be treated explicitly using electronic continuum correction (ECC) methodology by scaling ion charges q_i.[28] In this study, the simulations were performed using the parameters extensively benchmarked to reproduce the experimental uranyl-nitrate first and second association constants (K_1 and K_2) using the ECC methodology.[21] This methodology is performed on Joung et al. force fields for alkali metal ions[55] i.e. Li^+, Na^+ & Cs^+ by scaling the charges to 90 % of their original values to account for the polarization effects. Water is modeled using the TIP3P model in each simulated system.[56] The graphene layer was modeled and compared using the AMBER99[57] and CHARMM36[58] force fields. Both force fields exhibited similar behavior, and a detailed comparison is provided in the Supporting Information (SI). Amber99 force field for graphene is used in the final production runs. Non-bonded interactions were truncated to $r = 1.6$ *nm*. The particle mesh Ewald (PME) summation methodology is used for long-range electrostatic interactions.

Impact of ion charges on surface adsorption To probe the sensitivity of the ${UO_2}^{2+}$ adsorption towards the ion charges q_i, the charges on ${UO_2}^{2+}$, Li^+ and ${NO_3}^-$ were scaled from 80% to 95% (with an increment of 5%) of the initial Joung-Wipff combination of force fields.[55, 59, 60] We plotted the density of ${UO_2}^{2+}$ at the graphene surface varied with q_i. We observe a dependence of ion charge on the adsorption behavior of ${UO_2}^{2+}$ at the interface, which is directly related to an enhancement in ion association within the interfacial region, similar to what was previously observed at the hexane/electrolyte interface.[21] For each q_i, the normalized density profiles reveal a ${UO_2}^{2+}$ excess in the interfacial region, with a ${UO_2}^{2+}$ density 30 times greater than the bulk with no charge scaling, and 30 times greater density at 80% charge scaling (Figure S1). Recently, we demonstrated that a charge scaling factor of 0.9 (applied to Joung-Wipff et al. force fields) reproduced experimental ${UO_2}^{2+}$-${NO_3}^-$ association constants (in $LiNO_3$). To keep the consistency, we employed a charge scaling of 90% to the ion force fields in this study.[21]

Supplementary Information

System Configuration; Force fields benchmarking; Normalized density profiles, Average residence times, Density profiles of lithium complexes.

Acknowledgements

N.K. gratefully acknowledges the Center for Institutional Research Computing (CIRC) at Washington State University for providing computational resources. Financial support from the PNNL-WSU Distinguished Graduate Research Program is also acknowledged. N.K. extends sincere thanks to Prof. Dr. Aurora Clark and Dr. Bruce Moyer for their valuable discussions and insights regarding the content of this work.

Conflicts of Interest

None.

[1] Lu, Y. Coordination chemistry in the ocean. *Nature Chemistry* **2014**, *6*, 175–177.

[2] Ewing, R. C.; Weber, W. J.; Clinard Jr, F. W. Radiation effects in nuclear waste forms for high-level radioactive waste. *Progress in nuclear energy* **1995**, *29*, 63–127.

[3] Rao, T. P.; Metilda, P.; Gladis, J. M. Preconcentration techniques for uranium (VI) and thorium (IV) prior to analytical determination—an overview. *Talanta* **2006**, *68*, 1047–1064.

[4] Gu, B.; Ku, Y.-K.; Jardine, P. M. Sorption and binary exchange of nitrate, sulfate, and uranium on an anion-exchange resin. *Environmental science & technology* **2004**, *38*, 3184–3188.

[5] Wang, J.; Zhuang, S. Extraction and adsorption of U (VI) from aqueous solution using affinity ligand-based technologies: an overview. *Reviews in Environmental Science and Bio/Technology* **2019**, *18*, 437–452.

[6] Tsouris, C. Uranium extraction: fuel from seawater. *Nature Energy* **2017**, *2*, 1–3.

[7] Uysal, A. Aqueous interfaces in chemical separations. *Langmuir* **2023**, *39*, 17570–17580.

[8] Sisodiya, D. S.; Ali, S. M.; Chattopadhyay, A. Unexplored Isomerization Pathways of Azobis (benzo-15-crown-5): Computational Studies on a Butterfly Crown Ether. *The Journal of Physical Chemistry A* **2023**, *127*, 7080–7093.

[9] Zhao, G.; Wen, T.; Yang, X.; Yang, S.; Liao, J.; Hu, J.; Shao, D.; Wang, X. Preconcentration of U (VI) ions on few-layered graphene oxide nanosheets from aqueous solutions. *Dalton Transactions* **2012**, *41*, 6182–6188.

[10] Wu, Q.-Y.; Lan, J.-H.; Wang, C.-Z.; Xiao, C.-L.; Zhao, Y.-L.; Wei, Y.-Z.; Chai, Z.-F.; Shi, W.-Q. Understanding the bonding nature of uranyl ion and functionalized graphene: a theoretical study. *The Journal of Physical Chemistry A* **2014**, *118*, 2149–2158.

[11] Zong, P.; Wang, S.; Zhao, Y.; Wang, H.; Pan, H.; He, C.

Synthesis and application of magnetic graphene/iron oxides composite for the removal of U (VI) from aqueous solutions. *Chemical Engineering Journal* **2013**, *220*, 45–52.

[12] Deb, A.; Ilaiyaraja, P.; Ponraju, D.; Venkatraman, B. Diglycolamide functionalized multi-walled carbon nanotubes for removal of uranium from aqueous solution by adsorption. *Journal of Radioanalytical and Nuclear Chemistry* **2012**, *291*, 877–883.

[13] Fasfous, I. I.; Dawoud, J. N. Uranium (VI) sorption by multiwalled carbon nanotubes from aqueous solution. *Applied Surface Science* **2012**, *259*, 433–440.

[14] Maity, T.; Aggarwal, A.; Dasgupta, S.; Velachi, V.; Singha Deb, A. K.; Ali, S. M.; Maiti, P. K. Efficient Removal of Uranyl Ions Using PAMAM Dendrimer: Simulation and Experiment. *Langmuir* **2023**, *39*, 6794–6802.

[15] McCaffrey, D. L.; Nguyen, S. C.; Cox, S. J.; Weller, H.; Alivisatos, A. P.; Geissler, P. L.; Saykally, R. J. Mechanism of ion adsorption to aqueous interfaces: Graphene/water vs. air/water. *Proceedings of the National Academy of Sciences* **2017**, *114*, 13369–13373.

[16] Schwierz, N.; Horinek, D.; Netz, R. R. Reversed anionic Hofmeister series: the interplay of surface charge and surface polarity. *Langmuir* **2010**, *26*, 7370–7379.

[17] Cole, D. J.; Ang, P. K.; Loh, K. P. Ion adsorption at the graphene/electrolyte interface. *The Journal of Physical Chemistry Letters* **2011**, *2*, 1799–1803.

[18] Jungwirth, P.; Tobias, D. J. Specific ion effects at the air/water interface. *Chemical reviews* **2006**, *106*, 1259–1281.

[19] Jungwirth, P.; Tobias, D. J. Ions at the air/water interface. *The Journal of Physical Chemistry B* **2002**, *106*, 6361–6373.

[20] Vazdar, M.; Pluharova, E.; Mason, P. E.; Vácha, R.; Jungwirth, P. Ions at hydrophobic aqueous interfaces: Molecular dynamics with effective polarization. *The Journal of Physical Chemistry Letters* **2012**, *3*, 2087–2091.

[21] Kumar, N.; Servis, M. J.; Clark, A. E. Uranyl Speciation in the Presence of Specific Ion Gradients at the Electrolyte/Organic Interface. *Solvent Extraction and Ion Exchange* **2022**, *40*, 165–187.

[22] Hua, W.; Verreault, D.; Allen, H. C. Surface electric fields of aqueous solutions of NH4NO3, Mg (NO3) 2, NaNO3, and LiNO3: implications for atmospheric aerosol chemistry. *The Journal of Physical Chemistry C* **2014**, *118*, 24941–24949.

[23] Ganesan, P.; Kamaraj, R.; Vasudevan, S. Application of isotherm, kinetic and thermodynamic models for the adsorption of nitrate ions on graphene from aqueous solution. *Journal of the Taiwan Institute of Chemical Engineers* **2013**, *44*, 808–814.

[24] Kumar, N.; Servis, M. J.; Liu, Z.; Clark, A. E. Competitive interactions at electrolyte/octanol interfaces: A molecular perspective. *The Journal of Physical Chemistry C* **2020**, *124*, 10924–10934.

[25] Kumar, N.; Sadhu, B.; Clark, A. E. Essential Aspects of Solvent Effects and Solution Conditions upon the Modeling and Simulation of Lanthanide and Actinide Complexes. *Rare Earth Elements and Actinides: Progress in Computational Science Applications* **2021**, 249–276.

[26] Sala, J.; Guardia, E.; Martí, J. Specific ion effects in aqueous eletrolyte solutions confined within graphene sheets at the nanometric scale. *Physical Chemistry Chemical Physics* **2012**, *14*, 10799–10808.

[27] Williams, C. D.; Dix, J.; Troisi, A.; Carbone, P. Effective polarization in pairwise potentials at the graphene–electrolyte interface. *The journal of physical chemistry letters* **2017**, *8*, 703–708.

[28] Kirby, B. J.; Jungwirth, P. Charge scaling manifesto: A way of reconciling the inherently macroscopic and microscopic natures of molecular simulations. *The journal of physical chemistry letters* **2019**, *10*, 7531–7536.

[29] Chiang, K.-Y.; Seki, T.; Yu, C.-C.; Ohto, T.; Hunger, J.; Bonn, M.; Nagata, Y. The dielectric function profile across the water interface through surface-specific vibrational spectroscopy and simulations. **2022**,

[30] Lee, S. S.; Koishi, A.; Bourg, I. C.; Fenter, P. Ion correlations drive charge overscreening and heterogeneous nucleation at solid–aqueous electrolyte interfaces. *Proceedings of the National Academy of Sciences* **2021**, *118*, e2105154118.

[31] Uysal, A.; Zhou, H.; Feng, G.; Lee, S. S.; Li, S.; Fenter, P.; Cummings, P. T.; Fulvio, P. F.; Dai, S.; McDonough, J. K.; others Structural origins of potential dependent hysteresis at the electrified graphene/ionic liquid interface. *The Journal of Physical Chemistry C* **2014**, *118*, 569–574.

[32] Sangiovanni, D. G.; Faccio, R.; Gueorguiev, G. K.; Kakanakova-Georgieva, A. Discovering atomistic pathways for supply of metal atoms from methyl-based precursors to graphene surface. *Physical Chemistry Chemical Physics* **2023**, *25*, 829–837.

[33] Sfuncia, G.; Nicotra, G.; Giannazzo, F.; Pécz, B.; Gueorguiev, G. K.; Kakanakova-Georgieva, A. 2D graphitic-like gallium nitride and other structural selectivity in confinement at the graphene/SiC interface. *CrystEngComm* **2023**, *25*, 5810–5817.

[34] Zhou, H.; Uysal, A.; Anjos, D. M.; Cai, Y.; Overbury, S. H.; Neurock, M.; McDonough, J. K.; Gogotsi, Y.; Fenter, P. Understanding Defect-Stabilized Noncovalent Functionalization of Graphene. *Advanced Materials Interfaces* **2015**, *2*, 1500277.

[35] Lee, S. E.; Carr, A. J.; Kumal, R. R.; Uysal, A. Monovalent ion–graphene oxide interactions are controlled by carboxylic acid groups: Sum frequency generation spectroscopy studies. *The Journal of Chemical Physics* **2024**, *160*.

[36] Piontek, S. M.; Borguet, E. Vibrational Spectroscopy of Geochemical Interfaces. *Surface Science Reports* **2023**, 100606.

[37] Xu, M.; Liu, D.; Allen, H. C. Ethylenediamine at air/liquid and air/silica interfaces: protonation versus hydrogen bonding investigated by sum frequency generation spectroscopy. *Environmental science & technology* **2006**, *40*, 1566–1572.

[38] Zhan, C.; Cerón, M. R.; Hawks, S. A.; Otani, M.; Wood, B. C.; Pham, T. A.; Stadermann, M.; Campbell, P. G. Specific ion effects at graphitic interfaces. *Nature communications* **2019**, *10*, 4858.

[39] Greathouse, J. A.; O'Brien, R. J.; Bemis, G.; Pabalan, R. T. Molecular dynamics study of aqueous uranyl interactions with quartz (010). *The Journal of Physical Chemistry B* **2002**, *106*, 1646–1655.

[40] Kumar, N. Exclusive ion recognition using host–guest sandwich complexes. *Physical Chemistry Chemical Physics* **2024**, *26*, 3152–3158.

[41] Zarayeneh, N.; Kumar, N.; Kalyanaraman, A.; Clark, A. E. Dynamic Community Detection Decouples Multiple Time Scale Behavior of Complex Chemical Systems. *Journal of Chemical Theory and Computation* **2022**, *18*, 7043–7051.

[42] Kumar, N.; Clark, A. E. Unexpected inverse correlations and cooperativity in ion-pair phase transfer. *Chemical science* **2021**, *12*, 13930–13939.

[43] Neuefeind, J.; Soderholm, L.; Skanthakumar, S. Experimental coordination environment of uranyl (VI) in aqueous solution. *The Journal of Physical Chemistry A* **2004**, *108*, 2733–2739.

[44] Hagberg, D.; Karlström, G.; Roos, B. O.; Gagliardi, L. The coordination of uranyl in water: A combined quantum chemical and molecular simulation study. *Journal of the American Chemical Society* **2005**, *127*, 14250–14256.

[45] Suleimenov, O.; Seward, T. M.; Hovey, J. A spectrophotometric study on uranyl nitrate complexation to 150 C. *Journal of solution chemistry* **2007**, *36*, 1093–1102.

[46] Thompson, H. A.; Brown, G. E.; Parks, G. A. XAFS spectroscopic study of uranyl coordination in solids and aqueous solution. *American Mineralogist* **1997**, *82*, 483–496.

[47] Rao, L.; Tian, G. Thermodynamic study of the complexation of uranium (VI) with nitrate at variable temperatures. *The Journal of Chemical Thermodynamics* **2008**, *40*, 1001–1006.

[48] Zhang, Y.; de Aguiar, H. B.; Hynes, J. T.; Laage, D. Water structure, dynamics, and sum-frequency generation spectra at electrified graphene interfaces. *The journal of physical chemistry letters* **2020**, *11*, 624–631.

[49] Jiménez-Ángeles, F.; Harmon, K. J.; Nguyen, T. D.; Fenter, P.; de la Cruz, M. O. Nonreciprocal interactions induced by water in confinement. *Physical Review Research* **2020**, *2*, 043244.

[50] Gordillo, M.; Martí, J. Structure of water adsorbed on a single graphene sheet. *Physical Review B* **2008**, *78*, 075432.

[51] Ho, T. A.; Striolo, A. Polarizability effects in molecular dynamics simulations of the graphene-water interface. *The Journal of chemical physics* **2013**, *138*, 054117.

[52] Eslami, H.; Heydari, N. Hydrogen bonding in water nanoconfined between graphene surfaces: a molecular dynamics simulation study. *Journal of nanoparticle research* **2014**, *16*, 1–10.

[53] Abraham, M.; Murtol, T.; Schulz, R.; Pall, S.; Smith, J.; Hess, B.; Lindhal, E. GROMACS: High performance molecular simulations through multi-level parallelism from laptops to supercomputers. *SoftwareX* **2015**, *1-2*, 19–25.

[54] Martínez, L.; Andrade, R.; Birgin, E. G.; Martínez, J. M. PACKMOL: A package for building initial configurations for molecular dynamics simulations. *Journal of computational chemistry* **2009**, *30*, 2157–2164.

[55] Joung, I. S.; Cheatham III, T. E. Determination of alkali and halide monovalent ion parameters for use in explicitly solvated biomolecular simulations. *The journal of physical chemistry B* **2008**, *112*, 9020–9041.

[56] Jorgensen, W. L.; Chandrasekhar, J.; Madura, J. D.; Impey, R. W.; Klein, M. L. Comparison of simple potential functions for simulating liquid water. *The Journal of chemical physics* **1983**, *79*, 926–935.

[57] Hornak, V.; Abel, R.; Okur, A.; Strockbine, B.; Roitberg, A.; Simmerling, C. Comparison of multiple Amber force fields and development of improved protein backbone parameters. *Proteins: Structure, Function, and Bioinformatics* **2006**, *65*, 712–725.

[58] Vanommeslaeghe, K.; Hatcher, E.; Acharya, C.; Kundu, S.; Zhong, S.; Shim, J.; Darian, E.; Guvench, O.; Lopes, P.; Vorobyov, I.; others CHARMM general force field: A force field for drug-like molecules compatible with the CHARMM all-atom additive biological force fields. *Journal of computational chemistry* **2010**, *31*, 671–690.

[59] Guilbaud, P.; Wipff, G. Hydration of uranyl (UO22+) cation and its nitrate ion and 18-crown-6 adducts studied by molecular dynamics simulations. *The Journal of Physical Chemistry* **1993**, *97*, 5685–5692.

[60] Baaden, M.; Burgard, M.; Wipff, G. TBP at the water-oil interface: the effect of TBP concentration and water acidity investigated by molecular dynamics simulations. *The Journal of Physical Chemistry B* **2001**, *105*, 11131–11141.